Analyst

RSC Publishing

PAPER

View Article Online
View Journal | View Issue

Cite this: *Analyst*, 2013, **138**, 3230

Facile, sensitive, and ratiometric detection of mercuric ions using GSH-capped semiconductor quantum dots

Xianglong Zhu, Zhenghuan Zhao, Xiaoqin Chi and Jinhao Gao*

Received 3rd January 2013
Accepted 26th March 2013

DOI: 10.1039/c3an00011g

www.rsc.org/analyst

Glutathione (GSH) capped CdTe semiconductor quantum dots (QDs) are applied for detecting mercuric ions (Hg^{2+}) of trace quantity. The synthesis of GSH-capped CdTe (CdTe@GSH) QDs is cost-efficient and straightforward. We observed that Hg^{2+} can quantitatively quench the fluorescence of CdTe@GSH QDs and further induce the slight redshift of emission peaks due to the quantum confinement effect. Detailed studies by spectroscopy, dynamic light scattering (DLS), and electrospray ionization mass spectrometry (ESI-MS) demonstrated that the competitive Hg^{2+} binding with GSH makes the surface of CdTe QDs exposed, results in gradual aggregation, and quantitatively changes the photophysical properties of QDs. The whole procedure for detecting Hg^{2+} by this protocol took less than 10 min. The experimental limit of detection (LOD) of Hg^{2+} can be as low as 5 nM using CdTe@GSH with a low concentration (0.5 nM) because of the excellent fluorescent properties of QDs. This strategy may become a promising means to simply detect Hg^{2+} in water with high sensitivity.

Introduction

As a widely existing environmental pollutant, mercuric ion (Hg^{2+}) presents a serious threat to human health and the environment. Particularly, Hg^{2+} can be converted to the most toxic form of mercury (*i.e.*, methylmercury) by the action of anaerobic organisms, and finally concentrated in human bodies by biomagnification through the food chain.[1] Mercury poisoning has been related to several diseases associated with environmental pollution.[2] The U.S. Food and Drug Administration (FDA) set the safety limit of mercury in drinking water at 2 μg L^{-1} (~10 nM). Because of health concerns and legal restrictions, it is critical to develop probes which can detect Hg^{2+} with high sensitivity and selectivity. Suitable procedures include traditional atomic absorption spectrometry and atomic emission spectrometry. Recently, inductively coupled plasma mass spectroscopy (ICP-MS) and atomic fluorescence spectroscopy (AFS) have further increased the capability to determine low Hg^{2+} levels accurately.[3,4] However, these techniques require expensive and sophisticated instruments. For easier detection, a number of techniques and novel probes for detecting Hg^{2+} have been exploited over the past years.[5–8] Among the various methods reported, fluorescent dye sensors are widely used.[9,10] However, organic dyes often suffer from complicated synthesis and poor stability. We are still in need of appropriate methods for the detection of mercury contamination with low cost, high sensitivity, good stability, and ease of operation.

Quantum dots (QDs) are semiconductor nanoparticles generally composed of II–IV and III–V elements. They have many excellent optical properties such as high quantum yields (QYs), tunable size-dependent emission, and narrow emission peaks compared with their bulk materials and traditional organic dyes.[11–13] Recent advances in QDs have shown great promise in the detection of various metal cations besides Hg^{2+}.[14–17] For example, Dong *et al.* reported that the fluorescence intensity of mercaptopropionic acid (MPA)-coated CdS QDs was reduced selectively in the presence of Ag^{+}.[18] Gattas-Asfura and Leblanc also described the optical detection of Cu^{2+} and Ag^{+} with peptide-coated CdS QDs.[19] Liu *et al.* used CdTe QDs as Förster resonance energy transfer (FRET) donors to detect Hg^{2+}.[20] Recently, Han *et al.* reported that the mercaptosuccinic acid (MSA)–QD system can be a selective and sensitive method for detection of Hg^{2+}, and the limit of detection (LOD) was 0.6 μM.[21] However, these methods for detection of heavy metal ions based on QD systems are still immature in demand of improvements in selectivity, LOD, and the understanding of the quenching mechanism.

Glutathione (GSH) plays an important role in heavy metal detoxification in yeasts, bacteria, and plants, allowing the latter to grow in toxic soils. The possible reason is that the formation constant of the Hg^{2+}–thiol bond has been estimated to be as much as 10 orders of magnitude greater than the formation constant for the bonding of Hg^{2+} to nucleophiles present in the same environment.[22] Hg^{2+} has an extremely high affinity for thiol-containing biomolecules, such as GSH, cysteine, homocysteine, *N*-acetylcysteine, metallothionein, and albumin.[23] Based on this concept, we herein develop a rapid, convenient, sensitive, and reliable assay for Hg^{2+} detection using

State Key Laboratory of Physical Chemistry of Solid Surfaces, The Key Laboratory for Chemical Biology of Fujian Province, Department of Chemical Biology, College of Chemistry and Chemical Engineering, Xiamen University, Xiamen 361005, China. E-mail: jhgao@xmu.edu.cn; Fax: +86-592-2189959; Tel: +86-592-2180278

GSH-capped CdTe (CdTe@GSH) QDs (experimental LOD as low as 5 nM).

Experimental

Instrumentation and reagents

The fluorescence spectra were collected using a FluoroMax-4 Spectrofluorometer (HORIBA Jobin Yvon). TEM images were taken using a JEM-2100 microscope (JEOL). DLS data were recorded using a Zetasizer Nano ZS-90 granulometer (Malvern). The UV-Vis absorption was recorded with a UV-2550 UV-Vis spectrophotometer (Shimadazu). Mass spectrometric analysis was performed on an Esquire 3000 Plus instrument (Bruker).

Cadmium chloride (anhydrous), tellurium powder (30 mesh), chromium chloride hexahydrate, L-glutathione (GSH), and sodium borohydride were purchased from Alfa Aesar. Ferric chloride (anhydrous), ferrous chloride (anhydrous), manganese chloride tetrahydrate, mercury chloride, nickel chloride hexahydrate, and calcium chloride (anhydrous) were purchased from Sinopharm Chemical Reagent. PD-10 desalting columns containing Sephadex G-25 medium were purchased from GE Healthcare. Ultra-filtration was performed by Amicon Ultra 15 mL Filters with 50k MWCO (Merck Millipore). Milli-Q ultrapure water (18.2 MΩ cm) was used in all experiments.

Synthesis of CdTe@GSH QDs

CdTe@GSH QDs were synthesized according to a previously reported protocol with modification.[24] Briefly, to prepare NaHTe precursor solution, $NaBH_4$ (25 mg) was dissolved in H_2O (1 mL) and then mixed with tellurium powder (40 mg). The mixture was degassed followed by filling with N_2. The reaction mixture was left at room temperature for 3 h with a liquid seal pipe for releasing the byproduct H_2 until the solution turned purple.

To synthesize CdTe@GSH QDs, a 10 mL solution containing $CdCl_2$ (1.25 mM) and GSH (1.5 mM) was prepared and the pH was adjusted to 9.5 with NaOH (1 M). Then the solution was heated to 80 °C. Afterwards, the as-prepared NaHTe solution (20 μL) was quickly injected into $CdCl_2$–GSH solution with vigorous stirring. The reaction solution was then heated to 100 °C and refluxed to promote the growth of nanocrystals. QDs with redshifted emission wavelengths were obtained by prolonging the heating time. During the reaction, aliquots of solution were collected at different time points (3, 5, 10, 20, 30, 45, 55, 65, 80, 100, and 150 min, respectively) to obtain QDs with different colors.

Purification by size exclusion chromatography column and QD concentration determination

For purifying QDs, we washed the PD-10 column using 20 mL of 0.01 M HEPES (4-(2-hydroxyethyl)-1-piperazineethanesulfonic acid) buffer (pH = 7.56) to make sure the column was filled with buffer, then added pre-synthesized QD solution (volume no more than 1 mL). We collected the eluate with UV lamp lighting. The QD concentration was calculated according to a method reported by Peng and co-workers.[25]

Emission/absorption spectra and quantum yield determination

The emission spectra of the QDs were recorded using a Jobin Yvon FluoroMax-4 spectrofluorometer with 365 nm as an excitation wavelength. The QD absorption spectra were obtained with a Shimadazu UV-2550 UV-Vis spectrophotometer. Fluorescein was used as the standard for QY determination (the QY of fluorescein is 0.95 in 0.1 M NaOH). The QYs of CdTe@GSH QDs were calculated according to the following equation:

$$\varnothing_x = \varnothing_s \left(\frac{A_s}{A_x}\right)\left(\frac{\mathrm{Int}_x}{\mathrm{Int}_s}\right)\left(\frac{\eta_x}{\eta_s}\right)^2 \quad (1)$$

where $\varnothing$ is the QY, A is the absorbance at the excitation wavelength (460 nm), Int is the area under the emission peak and η is the refractive index of the solvent. The subscripts s and x denote the respective values of the standard and samples.

Detecting the concentration of Hg^{2+} and the selectivity analysis

We used QD563 as the probe due to its highest QY. We diluted the QD solution to different concentrations, and added a given volume of Hg^{2+} solution to obtain the mixture of QDs (concentrations of 0.5, 1.25, 2.5, and 5 nM) and Hg^{2+} (concentrations of 0, 5, 10, 25, 50, 75, 100, 125, 150, and 200 nM), respectively. The fluorescence spectra were collected with the emission range from 500 to 650 nm 10 min after mixing. The excitation wavelength was set at 365 nm. The methods for detecting the response of QDs to other ions (Fe^{3+}, Fe^{2+}, Mn^{2+}, Cr^{3+}, Zn^{2+}, Ni^{2+}, Ca^{2+}, Co^{2+}, Al^{3+}, SO_4^{2-}) were similar.

Mass spectrometric analysis of the Hg–GSH complex

We used ultra-filters (M_w cut off ~50 kDa) to wash and desalt the CdTe@GSH QDs with a concentration of 200 nM. We repeated the filtration twice to make sure the QDs were dissolved in pure water. After mixing the $HgCl_2$ and QD solutions, we did the ultra-filtration and diluted the filtrate 100-fold by 1 : 1 v/v water–methanol. Electrospray ionization mass spectrometry (ESI-MS) of the filtrate was performed using an Esquire 3000 Plus ion trap mass spectrometer in negative ion mode.

Results and discussion

Synthesis and characterization of CdTe@GSH QDs

The synthesis of GSH-capped QDs was adapted from a previously reported protocol with modification.[24] The reactions took place in three-neck flasks at the temperature of 100 °C. No complicated instruments or high-quality oxygen-free environments were required for the synthesis. A prolonged refluxing time promoted the growth of nanocrystals, which was accompanied by an increase in the emission wavelength from 500 to 680 nm with the fluorescence color ranging from cyan to red (Fig. 1a). CdTe@GSH QDs have similar QYs (Fig. 1b) with QDs synthesized with other water-soluble thiol-containing ligands, such as MPA and thioglycolic acid (TGA).[26–28] QDs with an emission peak at 563 nm (QD563) have the narrowest full width at half-maximum (FWHM) of the fluorescence spectrum

(48 nm) and the highest QY (40.3%) among CdTe@GSH samples (Fig. 1a and b), so we chose QD563 as the probe for detection and analysis of Hg^{2+}. The transmission electron microscopy (TEM) image illustrates that QDs possess good dispersion and have a mean core diameter of about 3.5 nm (Fig. 1c). Dynamic light scattering (DLS) analysis revealed that the hydrodynamic diameter (HD) of QD563 was 4.8 nm with a polydispersity index (PDI) of 0.045 (Table 1). The UV-Vis spectrum of QD563 shows that the wavelength of the first excitonic absorption peak is about 543 nm (Fig. 1d).

QD stability and determination of the QD concentration

The fluorescence intensity of CdTe@GSH QDs is sensitive to pH values in aqueous solution. We tested the fluorescence of QD563 in buffers with different pH values (Fig. 2). With the increment of pH, the fluorescence intensity of QD563 increased. QDs obtained by other procedures are always suffering from pH stability, including QDs formed in water and QDs synthesized in oil-phase and then transferred into water using thiol–carboxylic acid such as MPA, TGA, MUA (11-mercaptoundecanoic acid), and DHLA (dihydrogen lipoic acid).[29–33] The main reason is that the carboxyl of the ligand plays an important role in the QD surface stabilization: the carboxylic acid form ($-COO^-$) of carboxyl raises the stability of QDs in water. Carboxylic acid on the surface also has a synergistic chelation effect with –SH in order to decrease desorption of the ligand from the QD surface.[34,35] After comparison, we chose HEPES buffer with pH = 7.56 as the media for detection and analysis of Hg^{2+}.

Table 1 DLS analysis and aggregation observation of CdTe@GSH QDs in the presence of Hg^{2+}

Hg^{2+} concentration[a]	RFI (%)[b]	Diameter (nm)[c]	PDI
0 μM[d]	100	4.8	0.045
0.5 μM[d]	71.4	6.5	0.062
1.5 μM[e]	49.8	28.2	0.097
5.0 μM[e]	15.5	264.3	0.154
10 μM[f]	6.14	922.6	0.369

[a] Concentration of QDs was 12.5 nM. [b] Relative fluorescence intensity. [c] Average particle diameter by DLS analysis after 10 min mixing. [d] Clear and homogeneous yellow solution after storage for at least 1 week. [e] Orange precipitate after storage for 3 days. [f] Dark orange precipitate at the bottom of the vial after storage for 24 h.

The concentration of purified QD563 was calculated according to a method reported by Peng and co-workers.[25] The size of QD563 (D, nm) is calculated to be 3.16 nm using the equation:

$$D = (9.8127 \times 10^{-7})\lambda^3 - (1.7147 \times 10^{-3})\lambda^2 + (1.0064)\lambda - (194.84) \quad (2)$$

where λ (nm) is the wavelength of the first excitonic absorption peak of the corresponding sample (*i.e.*, 543 nm for the QD563 sample). Then ε (extinction coefficient per mole at the first excitonic absorption peak) is calculated to be 1.053×10^6 mol^{-1} by the equation:

$$\varepsilon = 10\,043(D)^{2.12} \quad (3)$$

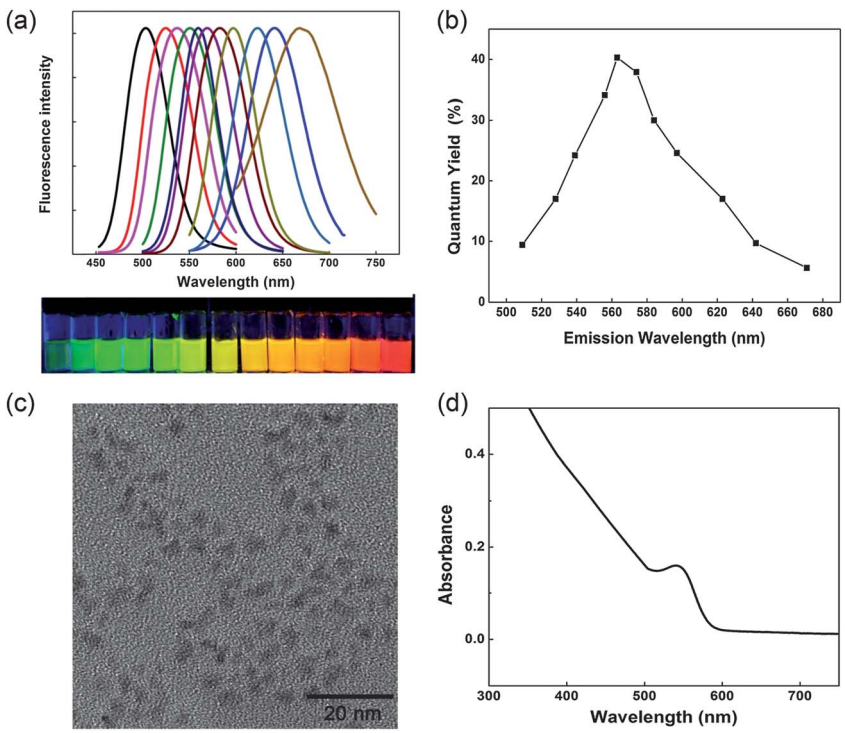

Fig. 1 (a) Fluorescence spectra (top) of CdTe@GSH QDs and photo (bottom) of the corresponding QDs with UV lamp irradiation (at 365 nm), the samples were collected at different reaction times (from left to right: 3, 5, 10, 20, 30, 45, 55, 65, 80, 100, and 150 min, respectively). (b) QYs of CdTe@GSH QDs with different emission wavelengths. (c) A representative TEM image of the QD563 sample. (d) Absorption spectrum of the purified QD563 sample.

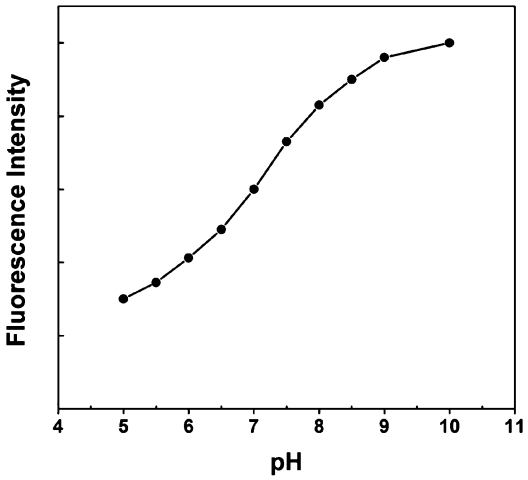

Fig. 2 Fluorescence intensity analysis of QD563 in buffers with different pH values: 0.05 M citric acid–sodium citrate buffer (pH 5.0); 0.02 M MES buffer (pH 5.5, 6.0, 6.5); 0.01 M HEPES (pH 7.0, 7.5, 8.0); 0.02 M Tricine buffer (pH 8.5); and 0.02 M Na_2CO_3–$NaHCO_3$ buffer (pH 9.0, 10.0).

The concentration of QD563 was finally obtained with calibrated absorbance using Lambert Beer's law.

Detection of Hg^{2+} of trace quantity

Using as-synthesized CdTe@GSH QDs (*e.g.*, QD563) as samples, we investigated the fluorescence changes after simple mixing of QD563 and Hg^{2+} solution. The fluorescence spectra show that the fluorescence intensity of CdTe@GSH QDs (1.25 nM) decreased by the increment of Hg^{2+} concentration, meanwhile, the slight redshift of the emission peak occurred during fluorescence quenching (Fig. 3a). In addition, little changes were found in fluorescence intensity after 10 min mixing, so this simple protocol allowed the detection of Hg^{2+} in solution within 10 min. Fig. 3b shows the comprehensive analysis of relative fluorescence intensity and maximum emission peak wavelengths of QDs at different Hg^{2+} concentrations. The fluorescence quenching efficiency is highly dependent on the concentration of Hg^{2+}, *i.e.*, higher Hg^{2+} concentration induces stronger fluorescence quenching of CdTe@GSH QDs. The redshift of emission peaks is up to 7 nm when the fluorescence is almost quenched.

We further studied the responsive capability of QDs with different concentrations. QDs with lower concentration had higher sensitivity to the same Hg^{2+} concentration (Fig. 4a). For instance, the 0.5 nM QD sample had good performance for Hg^{2+} detection from 5 nM to 75 nM, which is much lower than the 5 nM QD sample. Moreover, small distribution errors indicated that the fluorescence response to Hg^{2+} was highly reproducible, no matter what concentration of CdTe@GSH QDs was used (Fig. 4a). The fluorescence quenching is appropriately described by the Stern–Volmer equation:

$$I^0/I = 1 + K_{SV}[Q] \quad (4)$$

where [Q] is the concentration of the quencher (*i.e.*, Hg^{2+}) and K_{SV} is the Stern–Volmer constant. The linear relationship of the

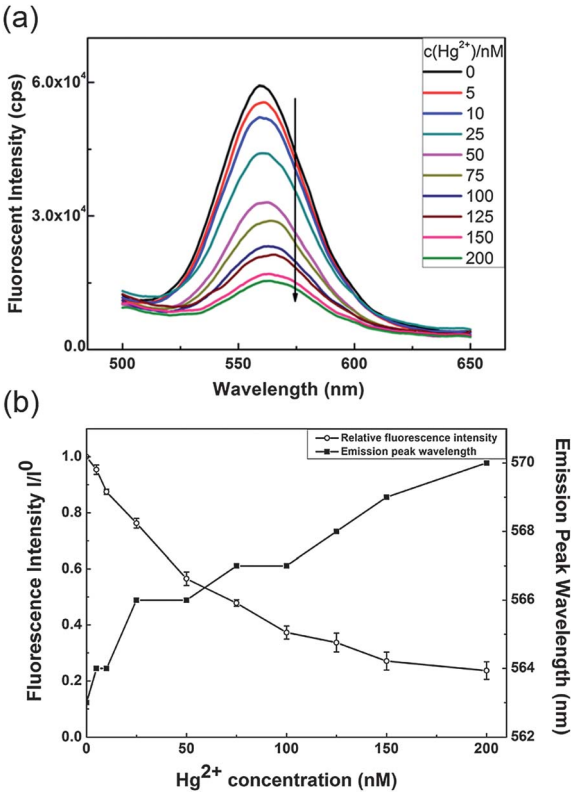

Fig. 3 (a) Fluorescence spectra of the QD563 (1.25 nM) sample with different concentrations of Hg^{2+} ions. (b) The analysis of relative fluorescence intensity changes and the redshift of emission peaks of QDs with different concentrations of Hg^{2+} ions.

Stern–Volmer plot of I^0/I *versus* Hg^{2+} concentration (Fig. 4b) suggests that a single class of fluorophores was equally accessible to all of the quenchers. So we can employ multiple samples to expand the detection range and optimize the detection conditions through selecting a sensor with a suitable concentration. The linear relationship ($R^2 = 0.9886$) between $1/K_{SV}$ and QD concentrations (Fig. 4c) and the linear relationship of the Stern–Volmer plot illustrate that this method is a ratiometric detection of Hg^{2+}. It is noted that $1/K_{SV}$ corresponds to the Hg^{2+} concentration when 50% of the fluorescence intensity was quenched. We could use extremely diluted QD samples to reach the low LOD of Hg^{2+}. According to eqn (4), it is calculated that we could observe 50% reduction of fluorescence intensity in the presence of 0.5 nM of Hg^{2+} (*i.e.*, $1/K_{SV} = 0.5$ nM) using CdTe@GSH QD solution with 0.1 nM concentration as the sensor, indicating that the LOD of Hg^{2+} could be as low as 0.5 nM.

The selectivity of Hg^{2+} detection by CdTe@GSH QDs

To verify the selectivity of CdTe@GSH QDs for detection of Hg^{2+}, we investigated the changes of QD fluorescence intensity in the presence of other interferential ions. CdTe@GSH QDs show no sensitivity to other metal or non-metal ions (Fe^{2+}, Fe^{3+}, Mn^{2+}, Cr^{3+}, Zn^{2+}, Ni^{2+}, Ca^{2+}, Co^{2+}, Al^{3+}, and SO_4^{2-}), even in the presence of the interferential ions with the concentration 50 times higher than Hg^{2+} (Fig. 5). The selective response of CdTe@GSH

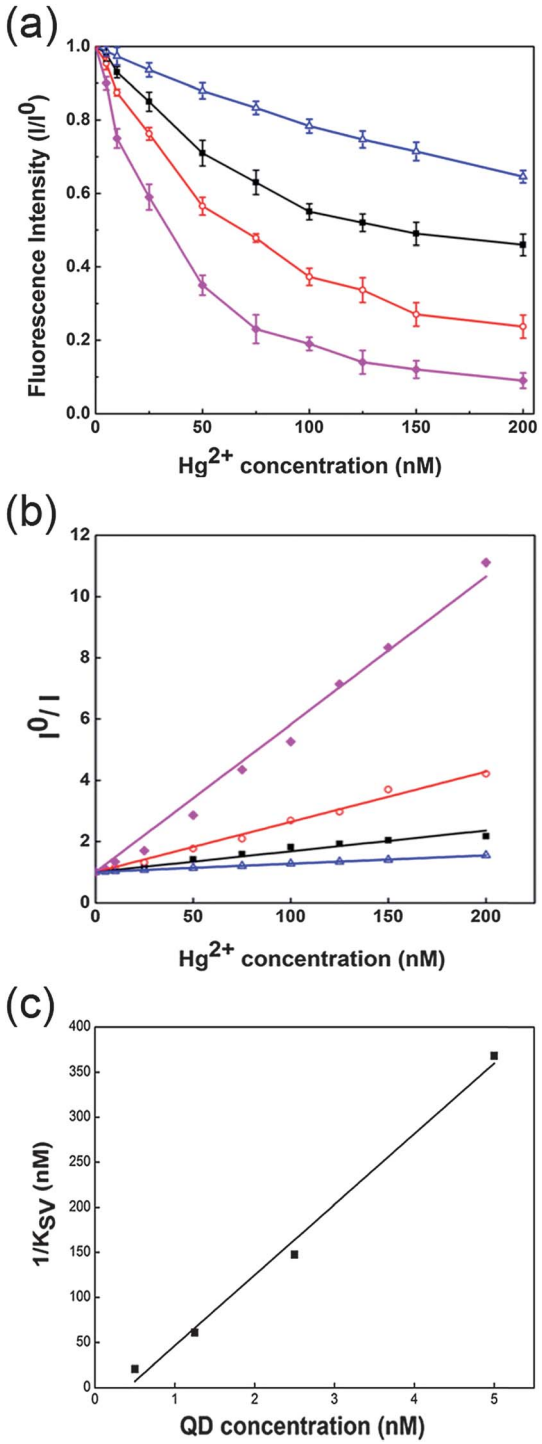

Fig. 4 (a) Effects of Hg^{2+} concentrations on the fluorescence intensity of QD563 with concentrations of (△) 5, (■) 2.5, (○) 1.25, and (◆) 0.5 nM in HEPES buffer (pH = 7.56). (b) Stern–Volmer plot of intensity changes corresponding to the concentrations of Hg^{2+} in (a). (c) Linear correlation of $1/K_{SV}$ values of QD563 with different concentrations. The excitation wavelength was 365 nm.

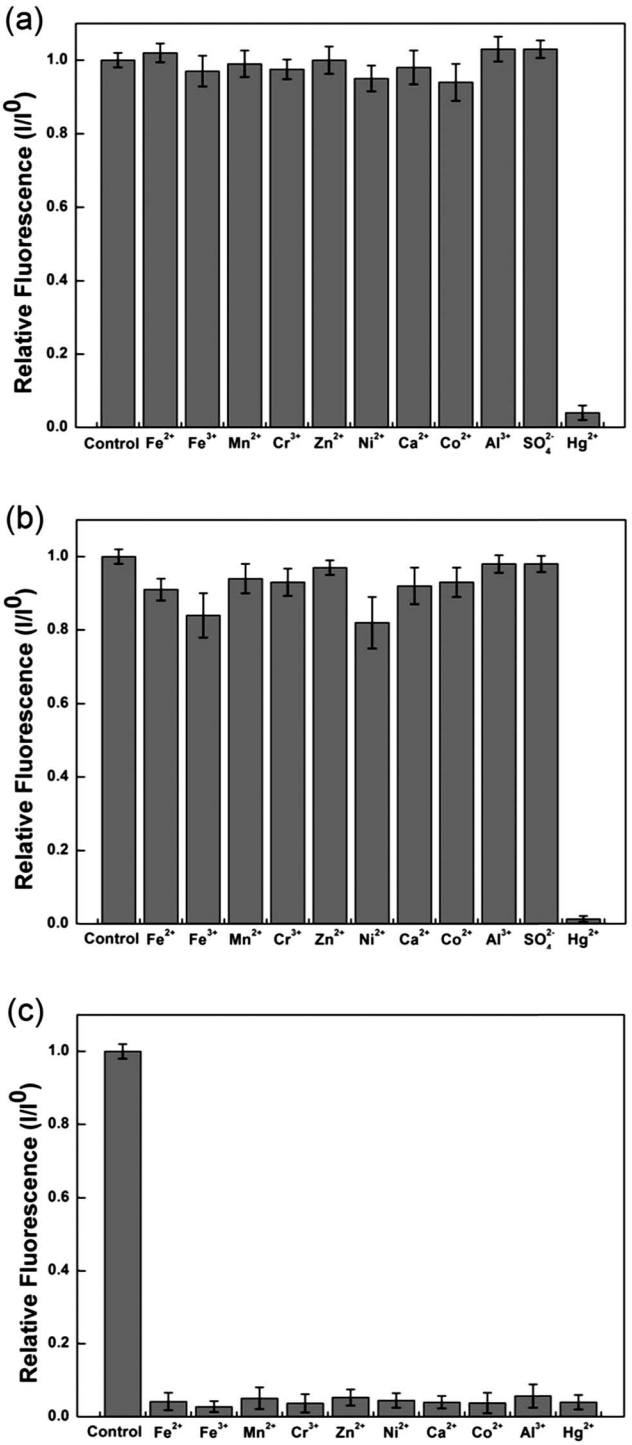

Fig. 5 Effect of different ions on the fluorescence intensity of 2.5 nM CdTe@GSH QD563. (a) The concentration of interferential ions and Hg^{2+} was 1 μM. (b) The concentration of interferential ions and Hg^{2+} was 50 μM. (c) Coexistence of Hg^{2+} (1 μM) and transition metal interferential ions (50 μM).

QDs suggests that Hg^{2+} plays a special role in fluorescence quenching, which may be helpful to understand the quenching mechanism. Moreover, the high selectivity of CdTe@GSH sensors to Hg^{2+} may be very useful in the analysis of complex samples.

Mechanism of Hg^{2+} detection by CdTe@GSH QDs

Accompanied by fluorescence quenching, we also found aggregation of QDs related to Hg^{2+} concentrations. Using DLS, we indeed observed the HDs of QDs changed along with the concentrations of Hg^{2+} (Table 1). QDs aggregated with the

increment of Hg^{2+} concentrations. The rise of PDI values suggested the inhomogeneity of aggregation. Moreover, precipitation of QDs occurred at high concentrations of Hg^{2+} ions (*e.g.*, 5 μM) after several days.

According to the previous reports, the mechanism of fluorescence quenching by Hg^{2+} is probably due to the metal ion displacement between Cd^{2+} (in QDs) and Hg^{2+} because of the high binding affinity of Hg^{2+} to Te^{2-} or Se^{2-}.[18,36] However, the formation of HgTe or HgSe (if happened) contributes to the fluorescence quenching of QDs or not still needs further investigation. In this study, the GSH capping layer is very important and crucial towards the quantum yield and water stability of QDs,[37] suggesting that the fluorescence quenching of QDs may be caused by the competitive GSH binding between the CdTe core and Hg^{2+} present in the solution.[38] Moreover, the binding energy of Hg^{2+} and S^{2-} ($K_{sp(HgS)} = 1.6 \times 10^{-52}$) is much more powerful than that of Cd^{2+} and S^{2-} ($K_{sp(CdS)} = 8.0 \times 10^{-27}$).[39] Therefore, we proposed that the GSH capping is preferentially displaced from the surface of QDs upon the binding of Hg^{2+} ions (in this case, other ions such as lead ($K_{sp(PbS)} = 8.0 \times 10^{-28}$) and copper ($K_{sp(CuS)} = 6.3 \times 10^{-36}$) may also bind to GSH because of their high binding affinity to thiol groups[40]). The displacement of GSH capping consequently creates imperfections on the QD surface, which causes the reduction of the quantum yield.[26] On the other hand, the loss of surfactant capping may lead to QD aggregation. These two causes can significantly result in fluorescence quenching.

To identify the competitive binding between Hg^{2+} and GSH, we detected the presence of a Hg–GSH complex in our experiments using ESI-MS. The analyte was the filtrate of the reacting mixture of CdTe@GSH and Hg^{2+} by ultra-filtration. As expected, we found the highest peak at 812.8 *m/z*, which corresponds to the formation of $[Hg(GSH)_2 - 3H]^-$. The ratio of the ion signal (*m/z*) range from 808 to 816 is consistent with the Hg–GSH complex species (Fig. 6, inset), conforming the formation of $Hg(GSH)_2$. Different from the reported Hg–GSH complex in ESI-MS spectra,[41,42] we did not observe obvious peaks of unsaturated Hg–GSH (*e.g.*, $[Hg(GSH) - 3H]^-$, *m/z* 506) or free GSH (*e.g.*, $[GSH - H]^-$, *m/z* 306; $[(GSH)_2 - 3H]^-$, *m/z* 611), which suggests that Hg^{2+} has so strong affinity with GSH and that all of the free Hg^{2+} was consumed. These results strongly support our proposal that Hg^{2+} takes GSH capping molecules away from the QD surface because of high affinity between Hg^{2+} and thiol groups in GSH.[38]

We also observed that the fluorescence quenching was always positively correlated with the emission wavelength redshift and the redshift was up to 7 nm when fluorescence was quenched to a very low level (Fig. 3b). According to the quantum confinement effect, fluorescence redshift is the sign of smaller band gap energy.[43,44] For the same semiconductor material, the increase of Exciton Bohr Radius (EBR) is the origin of reducing

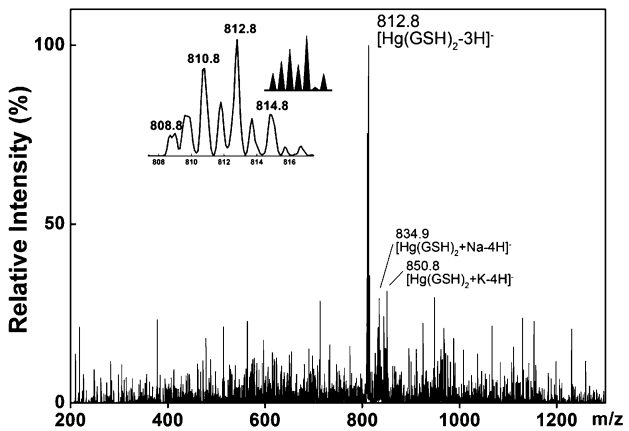

Fig. 6 Negative-ion source spectrum of the reaction mixture ultra-filtrated and 100-fold diluted in 1 : 1 v/v water–methanol. The inset shows details of the deprotonated molecule signal of $[Hg(GSH)_2 - 3H]^-$ and the calculated isotope pattern for the HgS_2 portion.

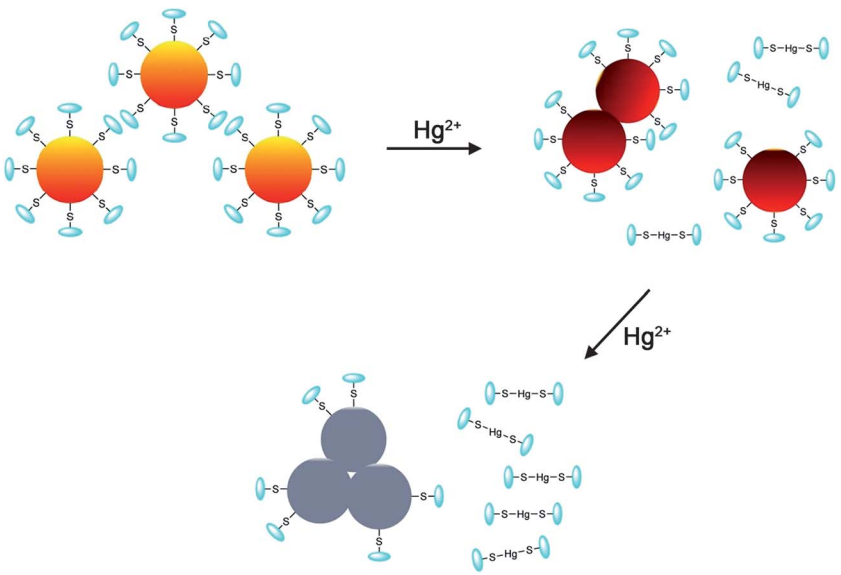

Fig. 7 Schematic illustration of the mechanism of CdTe@GSH QD fluorescence quenching in the presence of Hg^{2+}.

the quantum confinement effect and lowering the band gap energy.[45–48] The partial aggregation of uncapped QDs may induce the increase of EBR, which results in the redshift of emission wavelength. Less than 7 nm redshift is properly due to the very small contact area between the CdTe nanocrystals. Based on the phenomena mentioned above, we proposed the possible mechanism as shown in Fig. 7: Hg^{2+} takes GSH capping molecules away from the surface of CdTe QDs to form the $Hg(GSH)_2$ complex because of high affinity between Hg^{2+} and GSH. Then CdTe nanocrystals fuse together at the nude surface position to form dimer or trimer agglomerations, resulting in the redshift of emission wavelength and decrease of fluorescence intensity. With higher Hg^{2+} concentration, aggregation will be more serious, leading to the fluorescence quenching.

Conclusions

We have developed a simple and sensitive method to detect Hg^{2+} using CdTe@GSH QDs and elucidated the relationship between the Hg^{2+} concentration and fluorescence quenching of CdTe@GSH QDs. The calculated LOD of Hg^{2+} is as low as 0.5 nM based on the linear correlation of $1/K_{SV}$ using this detection protocol. We also proposed a reasonable and reliable mechanism about the fluorescence quenching of CdTe@GSH QDs based on the formation of $Hg(GSH)_2$ and detailed DLS analysis. The striping of GSH from the surface of nanoparticles causes QD aggregation, resulting in fluorescence quenching and emission peak redshift. This approach also has the capability to sensitively and selectively detect Hg^{2+} in the presence of the ionic mixture. The advantages of rapidity, reliability, high sensitivity, and selectivity make this method a promising way for detecting Hg^{2+} ions in environmental systems.

Acknowledgements

This work was partially supported by the National Key Basic Research Program of China (2013CB933901), the National Natural Science Foundation of China (21222106, 21021061, 81000662, and 81201805), the Fundamental Research Funds for the Central Universities (2010121012), the Scientific Research Foundation for the Returned Overseas Chinese Scholars and the Program for New Century Excellent Talents in University (NCET-10-0709).

References

1 *Toxicological Profile For Mercury*, US Department of Health and Human Services Public Health Service Agency for Toxic Substances and Disease Registry, 1999.
2 J. C. Clifton, *Pediatr. Clin. North Am.*, 2007, **54**, 237–269, viii.
3 N. Bloom and W. F. Fitzgerald, *Anal. Chim. Acta*, 1988, **208**, 151–161.
4 C. Haraldsson, S. Westerlund and P. Öhman, *Anal. Chim. Acta*, 1989, **221**, 77–84.
5 G. V. Ramesh and T. P. Radhakrishnan, *ACS Appl. Mater. Interfaces*, 2011, **3**, 988–994.
6 L. Chen, L. Yang, H. Li, Y. Gao, D. Deng, Y. Wu and L. J. Ma, *Inorg. Chem.*, 2011, **50**, 10028–10032.
7 M. H. Yang, P. Thirupathi and K. H. Lee, *Org. Lett.*, 2011, **13**, 5028–5031.
8 A. Singh, R. Pasricha and M. Sastry, *Analyst*, 2012, **137**, 3083–3090.
9 L. Wang, B. Zheng, Y. Zhao, J. Du and D. Xiao, *Anal. Methods*, 2012, **4**, 2369.
10 W. Xuan, C. Chen, Y. Cao, W. He, W. Jiang, K. Liu and W. Wang, *Chem. Commun.*, 2012, **48**, 7292–7294.
11 I. L. Medintz, H. T. Uyeda, E. R. Goldman and H. Mattoussi, *Nat. Mater.*, 2005, **4**, 435–446.
12 X. X. He, J. H. Gao, S. S. Gambhir and Z. Cheng, *Trends Mol. Med.*, 2010, **16**, 574–583.
13 X. Q. Chi, D. T. Huang, Z. H. Zhao, Z. J. Zhou, Z. Y. Yin and J. H. Gao, *Biomaterials*, 2012, **33**, 189–206.
14 E. M. Ali, Y. Zheng, H. H. Yu and J. Y. Ying, *Anal. Chem.*, 2007, **79**, 9452–9458.
15 H. Wang, Y. Li, X. Fei, L. Sun, L. Zhang, Z. Zhang, Y. Zhang, Y. Li and Q. Yang, *New J. Chem.*, 2010, **34**, 2996.
16 L. Cheng, X. Liu, J. Lei and H. Ju, *Anal. Chem.*, 2010, **82**, 3359–3364.
17 R. Freeman, T. Finder and I. Willner, *Angew. Chem., Int. Ed.*, 2009, **48**, 7818–7821.
18 C. Dong, H. Qian, N. Fang and J. Ren, *J. Phys. Chem. B*, 2006, **110**, 11069–11075.
19 K. M. Gattas-Asfura and R. M. Leblanc, *Chem. Commun.*, 2003, 2684.
20 B. Liu, F. Zeng, G. Wu and S. Wu, *Analyst*, 2012, **137**, 3717–3724.
21 B. Han, J. Yuan and E. Wang, *Anal. Chem.*, 2009, **81**, 5569–5573.
22 C. C. Bridges and R. K. Zalups, *Toxicol. Appl. Pharmacol.*, 2005, **204**, 274–308.
23 G. N. George, R. C. Prince, J. Gailer, G. A. Buttigieg, M. B. Denton, H. H. Harris and I. J. Pickering, *Chem. Res. Toxicol.*, 2004, **17**, 999–1006.
24 Y. Zheng, S. Gao and J. Y. Ying, *Adv. Mater.*, 2007, **19**, 376–380.
25 W. W. Yu, L. Qu, W. Guo and X. Peng, *Chem. Mater.*, 2003, **15**, 2854–2860.
26 C. Park and T. H. Yoon, *Colloids Surf., B*, 2010, **75**, 472–477.
27 Y. F. Liu and J. S. Yu, *J. Colloid Interface Sci.*, 2009, **333**, 690–698.
28 J. Tian, R. Liu, Y. Zhao, Q. Xu and S. Zhao, *J. Colloid Interface Sci.*, 2009, **336**, 504–509.
29 J. Moon, K.-S. Choi, B. Kim, K.-H. Yoon, T.-Y. Seong and K. Woo, *J. Phys. Chem. C*, 2009, **113**, 7114–7119.
30 N. A. Al-Hajaj, A. Moquin, K. D. Neibert, G. M. Soliman, F. M. Winnik and D. Maysinger, *ACS Nano*, 2011, **5**, 4909–4918.
31 Y. Yu, L. Xu, J. Chen, H. Gao, S. Wang, J. Fang and S. Xu, *Colloids Surf., B*, 2012, **95**, 247–253.
32 H. S. Choi, W. Liu, P. Misra, E. Tanaka, J. P. Zimmer, B. Itty Ipe, M. G. Bawendi and J. V. Frangioni, *Nat. Biotechnol.*, 2007, **25**, 1165–1170.

33 I. L. Medintz, A. R. Clapp, H. Mattoussi, E. R. Goldman, B. Fisher and J. M. Mauro, *Nat. Mater.*, 2003, **2**, 630–638.
34 H. Zhang, Z. Zhou, B. Yang and M. Gao, *J. Phys. Chem. B*, 2003, **107**, 8–13.
35 L. Shang, L. Zhang and S. Dong, *Analyst*, 2009, **134**, 107–113.
36 J. G. Liang, X. P. Ai, Z. K. He and D. W. Pang, *Analyst*, 2004, **129**, 619–622.
37 J. M. Klostranec and W. C. W. Chan, *Adv. Mater.*, 2006, **18**, 1953–1964.
38 B. J. Fuhr and D. L. Rabenstein, *J. Am. Chem. Soc.*, 1973, **95**, 6944–6950.
39 J. A. Dean, *Lange's Handbook of Chemistry*, McGraw-Hill Professional, 15th edn, 1998.
40 C. V. Durgadas, V. N. Lakshmi, C. P. Sharma and K. Sreenivasan, *Sens. Actuators, B*, 2011, **156**, 791–797.
41 N. Burford, M. D. Eelman and K. Groom, *J. Inorg. Biochem.*, 2005, **99**, 1992–1997.
42 F. M. Rubino, C. Verduci, R. Giampiccolo, S. Pulvirenti, G. Brambilla and A. Colombi, *J. Am. Soc. Mass Spectrom.*, 2004, **15**, 288–300.
43 W. E. Buhro and V. L. Colvin, *Nat. Mater.*, 2003, **2**, 138–139.
44 C. A. Leatherdale, W. K. Woo, F. V. Mikulec and M. G. Bawendi, *J. Phys. Chem. B*, 2002, **106**, 7619–7622.
45 C.-J. Lee, A. Mizel, U. Banin, M. L. Cohen and A. P. Alivisatos, *J. Chem. Phys.*, 2000, **113**, 2016.
46 A. J. Nozik, *Inorg. Chem.*, 2005, **44**, 6893–6899.
47 M. Brun, S. Huant, J. C. Woehl, J. F. Motte, L. Marsal and H. Mariette, *Solid State Commun.*, 2002, **121**, 407–410.
48 R. S. Silva, F. Qu, A. M. Alcalde and N. O. Dantas, *Microelectron. J.*, 2003, **34**, 647–649.